STRESS AND MODAL ANALYSIS OF A ROTATING BLADE AND THE EFFECTS OF NONLOCALITY

M. Tufekci*, Q. Rendu, J. Yuan, J.P. Dear, L. Salles
Department of Mechanical Engineering, Imperial College London
Exhibition Road, South Kensington Campus
London SW7 2AZ, UK
Email: m.tufekci17@imperial.ac.uk

A.V. Cherednichenko
Department of Applied Mathematics
Bauman Moscow State Technical University
2/18 Rubtsovskaıa Ul., Moscow 105005
Russian Federation

ABSTRACT

This study focuses on the quasi-static stress and modal analyses of a rotor blade by using classical and nonlocal elasticity approaches. The finite element method with an additional numerical integration process is used to evaluate the integral equation of nonlocal contionuum mechanics. The blade is assumed to be made of a linear elastic material of weak nonlocal characteristic. Such materials can be composites, metallic foams, nanophased alloys etc. A full-scale fan blade model is chosen as the test case to represent the rotor blade for a modern high bypass ratio turbofan engine. The boundary conditions and loads are chosen based on the steady-state cruising operating conditions of such blades. The nonlocal stresses are calculated by processing the calculated local stresses. To calculate the nonlocal stresses, the integral form of nonlocal elasticity is employed in the discretised domain. The results of the two cases are compared and discussed.

NOMENCLATURE

CAD Computer-aided drawing
3D Three dimensional
u Displacement
$\dot{u}$ Velocity
α Nonlocal modulus
γ Nonlocal constant
τ Nonlocal constant
a Intrinsic length
l Extrinsic length
σ Stress
ε Strain
e_0 Nonlocal material constant
Ω Infinite domain
V Finite domain
rpm Revolutions per minute
C_{ijkl} Stiffness tensor
SS Suction side
PS Pressure side
F Flapping mode
T Torsional mode
CW Chrodwise mode

Superscripts

nl Nonlocal
l Local

INTRODUCTION

The idea of using power without humans being involved in its generation is an idea which has been chased after starting from ancient times. Aeolipile of Heron is one of the ancestors of steam powered mechanisms. Furthermore, windmills and watermills use the power of wind and water stream to mill the grains.

Later, almost two centuries back from today, internal combustion engines stepped onto the stage and dominated power generation. Nearly in the same period of time, engineers and scientists started work on one of the most common power generation methods nowadays, turbines engines. While the future of the internal combustion engines is in discussion, with a promising future, gas turbines engines still attract attention so that even nanoturbines are being researched [1].

As the first component of a gas turbine engine, the fan is crucial. The fan is responsible for the air intake, which is directly related to the efficiency of the engine. Furthermore, the fan contributes to 80% of the thrust generated by the engine [2]. Increasing the radius of the fan also increases the thrust [3]. Seeking for more thrust brings problems with it. The geometry of the fan blade must satisfy conditions in two different fields, aerodynamics and solid mechanics. The blade must be long and slender to provide more thrust and better efficiency while being able to withstand the loads acting on it which are aerodynamic loads, centrifugal loads and contact at the tip and at the root in steady-state conditions [4–6]. Therefore, the design of the geometry of the rotor blades is a multidisciplinary iterative process [7, 8]. The blades are primarily designed and formed based on aerodynamic or similar fluid dynamics calculations. Then the designs are checked with structural analysis. There are different structural modelling techniques for the blades. Based on the geometry the first technique that comes to mind is to model the blade as a shell [9]. But in some cases, shells introduce relatively complicated expressions to be solved and usually, they are computationally expensive. Hence, a simpler structure is used as an alternative modelling method, namely beams [10, 11]. However, simple beam formulations may not be accurate enough for a detailed fan blade modelling. Thus, beam formulations are modified to increase the accuracy of the representation of blades by taking the thin-walled structure of the blades into account [12]. Furthermore, reduced-order modelling is another modelling technique that is applied to the fan blades as well [13]. Even though there is research to do improvements on the fan blade geometry, it is a fact that the shape of the blade is restricted [14]. The reason for the restriction of the geometry, the design of the blade is mainly controlled by the fluid flow. So, the design should not disturb the flow which would lead to reduction thrust and efficiency. Hence, the design does not offer much flexibility for solid mechanics part of the system design.

With restricted geometry, engineers tend to do research on improvement on the materials for the rotor blades [15]. Traditional metallic materials are limited for further improvements in weight reduction and aerodynamic performance on rotor blades with significant centrifugal loads. Larger densities of materials cause large stresses in rotating parts. Therefore, higher specific strengths are required from the material. Whereas modern engineering materials such as foams and composites have much more flexible and tailorable mechanical properties, relatively better specific strength and lightweight in comparison to the traditional materials [16, 17]. However, mechanical modelling of those modern materials might require more advanced techniques than classical continuum theory, due to their nonhomogeneous internal structures [18, 19]. The internal structure of such modern materials is usually inhomogenous. They are either composed of multiple materials/phases and/or include cavities. Utilising different materials in the same structure helps to reduce the weight without losing much of stiffness and strength. Whereas cavity inclusion might increase the stiffness and strength of the material under certain conditions with strain hardening mechanism [20].

Those inhomogeneities limit the capabilities of the classical continuum theory to handle the media as bulk and homogeneous materials. Classical continuum theory essentially uses a volume element to derive the equilibrium equations involving stresses, body forces and inertial loads where this volume element is infinitesmal. Whereas in composites or foams, the volume element has a minimum size to be representative [21]. This brings out the need to have a scale dependency for a continuum theory since the classical theory has no consideration of the scale [22]. Mindlin is one of the first researchers who claimed the scale effect influences the material behaviour [23]. This is followed by the formulation of another advanced continuum theory evaluating the scale effect in atomic/molecular scale. This is called as the nonlocal continuum theory developed by A. Cemal Eringen [24]. Nonlocal continuum theory is one of the most advanced continuum theories in the literature that are successful in modelling such inhomogenous media with good accuracy [25]. One important thing to note about the nonlocal continuum theory applied on micro/nano continua, it is possible to validate the results of nonlocal continuum theory with other methods such as molecular dynamics [26, 27].

To formulate accurately representative structures using nonlocal continuum theory is harder in comparison to the classical continuum theory. This is mainly because of the introduction of complexities by the fundamental nonlocal integral equation. Therefore, it more common to work with simpler formulations such as beams, plates and shells [28–31]. To solve those formulations, usually numerical methods are employed such as finite element method [32]. It is also possible to derive specific element formulations for relatively more complicated cases the same way it is used for classical applications with the nonlocal terms added [19, 33–35].

This study looks into a problem of 3D quasi-static stress analysis of a fan blade structure using finite element method. A full-scale fan blade model is chosen as the test case to represent the rotor blade for a modern high bypass ratio turbofan engine. The blade is considered to be made of an isotropic, linear elastic material of weak nonlocal characteristic. The loads and the boundary conditions are arranged so that they are representative of steady-state operating conditions. The stress analysis of the nonlocal blade is done in two main steps. The first step is the

calculation of local stresses in the blade with the classical finite element procedure. Following this, in the second step the local stresses are postprocessed and the nonlocal stress components are calculated by numerical evaluation of the integral equation of nonlocal continuum theory. The local stress components of each point in the blade multiplied with the nonlocal kernel function and integrated over the domain. The results of local and nonlocal stresses are compared as well as the natural frequencies. Even though the industrial applications of such materials do not currently exist, nanocomposites, nanophased alloys or any other material which is likely to have nonlocal behaviour, might become usable in the future [36, 37].

MODELLING OF THE BLADE

A finite element study is conducted to model the behaviour of the representative blade structure. The modelling process starts with the generation of the CAD which is followed by meshing and preprocessing. Finally, the analysis is run and the stresses displayed and also exported for further postprocessing. This section describes this part of the study in some details. The flowchart shown in Fig. 1 summarises the strategy.

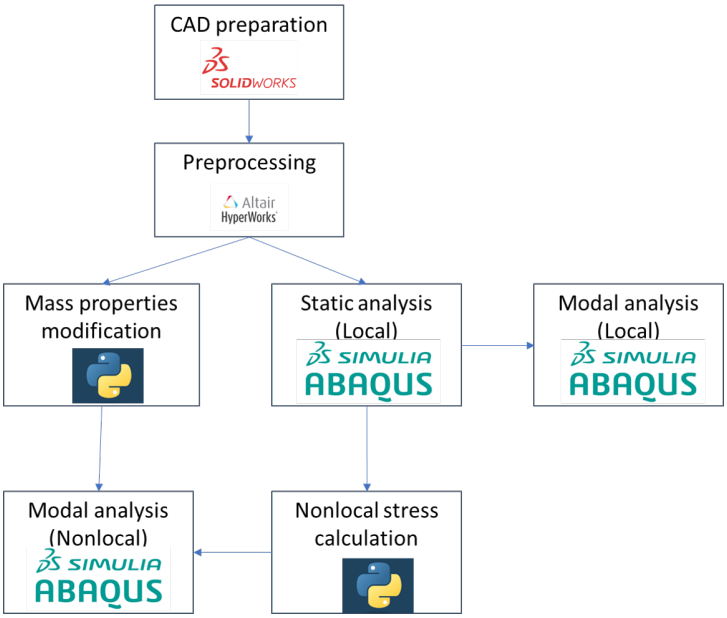

FIGURE 1. A SCHEMATIC OUTLINE OF THE STUDY

Finite Element Modelling of the Blade

Modelling of the blade starts with preparing the CAD. The overall geometry and the main dimensions are kept similar to a real fan blade which is as shown in Fig. 2. Hence, it is expected to be a representative solid model. The CAD is drawn in Solidworks and exported in universal CAD formats for further processing in the finite element softwares. The prepared solid model is shown in Fig. 3. The blade and the disc are considered as a single body system for the sake of simplicity to remove contact nonlinearities from the system. The contact introduces friction to the system. This changes the static stress and displacements significantly. Hence it is also to be stated the dynamic behaviour is also affected dramatically [5].

FIGURE 2. A FAN ASSEMBLY OF TRENT 500 DISPLAYED IN DEPARTMENT OF MECHANICAL ENGINEERING AT IMPERIAL COLLEGE LONDON

Following the preparation of the solid model, the CAD data is migrated to the software Hypermesh for mesh generation. Since the geometry is relatively complicated, quadratic tetrahedral elements are used to mesh the structure. 47 419 elements and 78 266 nodes are generated as the result of the meshing process. Doubling the node numbers, increased the stress levels by up to 3%. Therefore, it is judged that convergence is achieved. Taking note that the shear behaviour is to be captured by inserting two rows of quadratic elements throughout the blade thickness. Fig. 4 displays the final mesh. Pre-processing is done in the same software. The material is taken as a titanium alloy Ti-6Al-

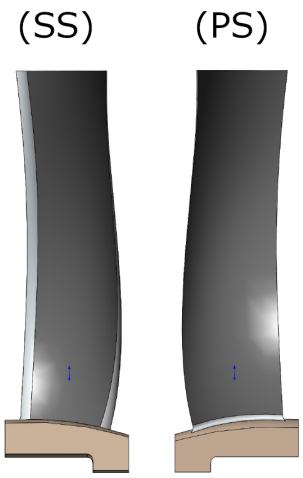

FIGURE 3. CAD MODEL OF THE BLADE

4V, which has the elastic modulus of 110 GPa, Poisson's ratio of 0.31 and the density of 4600 kg/m^3. The boundary conditions and the loads are selected so that they represent the steady-state operating conditions with caution. Hence, the rotational speed is taken as 2000 rpm. The steady-state aerodynamic loads consist of the pressure, due to the airflow. The aerodynamic pressure distribution is calculated by using CFD computations.

FIGURE 4. BLADE MODEL AFTER MESH PROCESSING

Static pressure on the blade surface is obtained through steady Reynolds-Averaged Navier-Stokes (RANS) computations. The software relies on edge-based finite-volume method to solve 3D compressible RANS equations on unstructured grids with Spalart-Allmaras turbulence model [38]. The chosen operating point corresponds to peak efficiency of the low-speed fan at the nominal rotational speed. The pressure distribution on the pressure side is given in Fig. 5.

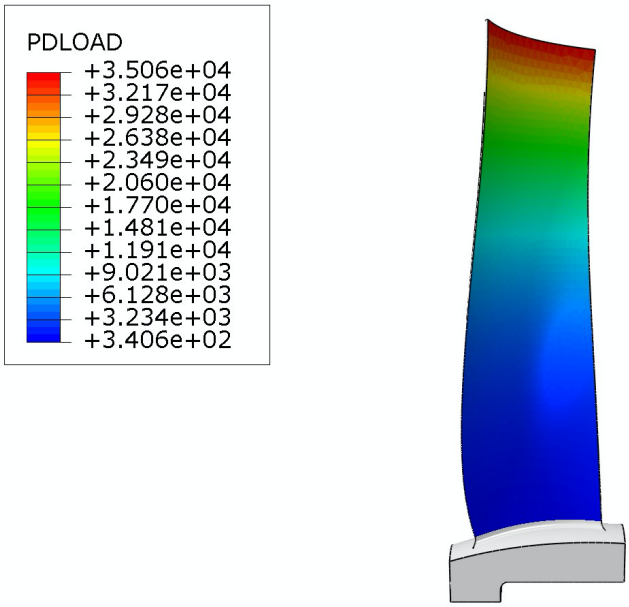

FIGURE 5. PRESSURE DISTRIBUTION ON THE PRESSURE SIDE (UNITS IN [Pa])

Cyclic symmetry is applied at the boundaries of the disc sector [39].

After preprocessing is done, the model is exported from Hypermesh and imported to Abaqus. Using Abaqus, a static analysis is run to obtain the stresses in the blade. The obtained results are visualised and exported for further processing. The exported stress data is used to calculate the nonlocal stress components.

For the modal analysis, the prestressed model is put through the procedure and natural frequencies and mode shapes are obtained. The effect of stress on natural frequencies is investigated.

NONLOCAL CONTINUUM THEORY

The nonlocal continuum theory assumes that the stresses of the individual points depend on the strains of all the points that lie within the whole domain. This dependency is defined over a kernel/attenuation function which peaks when the distance between the points are zero and approaches to infinity when the distance between the points increase. There are three essential constants to define the attenuation function: material constant, intrinsic and extrinsic lengths. This section covers basic details of the nonlocal continuum theory applied within the scope of this

study, some details of the attenuation function and how it is to be chosen as well as the calculation of inertial properties.

Integral Form of Nonlocal Elasticity

To explain the nonlocal elasticity theory it is a good start to give the relation between the classical elasticity and nonlocal elasticity in cartesian coordinates [26]. In Equation 1, the stress-strain relation of a linear elastic material within the boundaries of the classical theory of elasticity is given. The relation between the local and the nonlocal elasticity theories is given in the Equation (2).

$$\sigma^{\,l}_{ij} = C_{ijkl}\varepsilon^{l}_{kl} \tag{1}$$

$$\sigma^{nl}_{ij}(\mathbf{x}) = \int_{\Omega} \alpha_{ijkl}\left(\mathbf{x},\mathbf{x}^{'},\tau\right)\ \varepsilon^{l}_{kl}(\mathbf{x})\ d\Omega \tag{2}$$

In this equation, C_{ijkl} represents the stiffness tensor of the fourth-order, $\sigma^{\,l}_{ij}$, the local stress tensor, $\sigma^{\,nl}_{ij}$, the nonlocal stress tensor, ε_{ijkl} represents the classical/local strain tensor and α_{ijkl} a kernel tensor of the fourth order from which the kernel function is to be built. Also, $\mathbf{x}^{'}$,$\mathbf{x}$ are the field points and the points of interest respectively. These concepts are used in the definition of the kernel function, which is handled in the following section. The superscripts *nl* and *l* refer to nonlocal and local respectively. In isotropic continua, it is possible to distribute the kernel tensor uniformly to the components of the stiffness tensor and a scalar function remains as a factor within the integral. This is called the kernel function. Executing the distribution, the equation becomes as shown in the Equation (3).

$$\sigma^{nl}_{ij}(\mathbf{x}) = \int_{\Omega} \alpha\left(\mathbf{x},\mathbf{x}^{'},\tau\right)\ C_{ijkl}\varepsilon^{l}_{kl}\left(\mathbf{x}^{'}\right)\ d\Omega \tag{3}$$

Here C_{ijkl} represents the stiffness tensor of an isotropic and linear elastic material whereas α becomes the scalar kernel function. Combining the Equations (1) and (2) we get the relation between the local and nonlocal stresses for a linear elastic material. The form in the Equation (4) is obtained. This is called the integral form of nonlocal elasticity [26].

$$\sigma^{nl}_{ij}(\mathbf{x}) = \int_{\Omega} \alpha\left(\mathbf{x},\mathbf{x}^{'},\tau\right)\ \sigma^{l}_{ij}\left(\mathbf{x}^{'}\right)\ d\Omega \tag{4}$$

This integral is evaluated for each point of interest by scanning the entire domain. The point of interest ($\mathbf{x}$) is fixed while the points of the field ($\mathbf{x}^{'}$) are floating and so the field is scanned. During this scanning process, for each field point, the distance between the point of interest and the field point is calculated and used as input for the evaluation of the integral. The numerical evaluation of the integral is shown in Fig. 6.

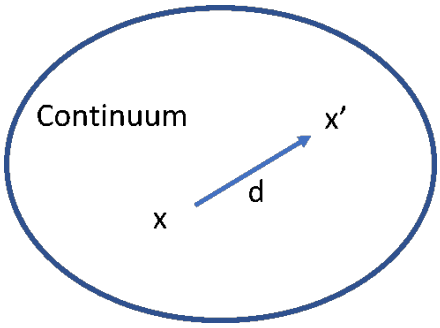

FIGURE 6. SCHEMATIC EVALUATION OF THE INTEGRAL

The Kernel Function and its Constants

Kernel function also called as the attenuation function, is the key of nonlocal continuum theory. It is defined as a function of the distance between field points, which are noted as $\mathbf{x}^{'}$, and the point of interest which are noted as $\mathbf{x}$, as well as the media itself. So the value of α changes while scanning the domain for integration, as it depends on the distance between points. Moreover, structural characteristics also have a dominant effect on the function. Those structural factors can be summarised as follows:

γ : Size parameter
e_0 : Material constant
a : Characteristic intrinsic length
l : Extrinsic length
τ : Nonlocal constant

Some of those concepts have relations which are shown in Equations (5) and (6).

$$\gamma = e_0 a \tag{5}$$

$$\tau = \gamma/l = e_0(a/l) \tag{6}$$

The nonlocal function α must satisfy the conditions below:

- When $\tau \longrightarrow 0$, α must converge to the form of a Dirac delta function, which means the local and nonlocal elasticity theories converge to each other and calculate the same results for the same cases.
- Nonlocal tensor shows symmetry with respect to the field $\mathbf{x}$.
- The nonlocal modulus reaches its peak where $\mathbf{x} = \mathbf{x}^{'}$ and approaches to 0 as the distance between the point and the field points increase.
- In an infinite space domain Ω, the integral of α in the domain is equal to 1. This is called the normalisation condition and is shown in Equation (7).

$$\int_{\Omega} \alpha \left(\mathbf{x}, \mathbf{x}^{'}, \tau\right) \, d\Omega = 1 \tag{7}$$

- If calculations are to be done in a finite domain V which is embedded in Ω, the normalisation condition turns out to the way shown in Equation (8).

$$\int_{\Omega} \alpha \left(\mathbf{x}, \mathbf{x}^{'}, \tau\right) \, dV' = 1 \tag{8}$$

Some of the constants of the kernel function, as mentioned earlier, are material dependent and known, such as e_0. But a and l are to be chosen based on the structure. The nonlocal constants in this equation are chosen taking care of the normalisation constant.

This normalisation condition alongside the limit condition of the kernel function, when the distance goes to infinity, $\tau \longrightarrow 0$ also leads to a practical concept. A radius can be defined where the nonlocal function has a significant effect on the actual stresses.

In this study, the extrinsic length is chosen as the average thickness of the blade, which is around 5 mm. Therefore l is assumed to be 5 mm. Since, in the scope of this paper, no specific material is handled, the nonlocal size parameter γ is used in the calculations, which is the multiplication of the intrinsic length a and the material constant e_0. The chosen attenuation function, which is a Gaussian function, is given in the Equation (9) [40]. It is also to be noted that the attenuation function has the dimensions of $force * length^{-5}$.

$$\alpha \left(\mathbf{x}, \mathbf{x}^{'}, \tau\right) = \frac{1}{2\gamma} \mathrm{e}^{-\frac{(|\mathbf{x}-\mathbf{x}^{'}|)^2}{l^2}} \tag{9}$$

Calculation of Inertial Properties and Nonlocal Stresses

Proceeding to the mass/inertia properties, inertia terms are modified by generating the relevant nonlocal component and summing it with the classical local inertial terms [23, 41]. Kinetic energy per unit volume T is expressed in Equation (10).

$$T = \frac{1}{2}\rho \dot{u}_j^l \dot{u}_j^l + \frac{1}{2V'} \int_{V'} \rho^{nl} \dot{u}_j^n l \dot{u}_j^n l dV' \tag{10}$$

Here ρ is the density of the material and $\dot{u}$ is the velocity in local and nonlocal theories to be distinguished based on the superscripts. The relation between local and nonlocal components of the density is given in Equation (11).

$$\rho^{nl} = \rho^l \gamma^2 \tag{11}$$

Plugging this relation into the Equation (10).

$$T = \frac{1}{2}\rho \dot{u}_j^l \dot{u}_j^l + \frac{1}{2V'} \gamma^2 \int_{V'} \rho^l \dot{u}_j^n l \dot{u}_j^n l dV' \tag{12}$$

As the next step, the total energy is to be calculated by integrating through the finite domain V. That integration is formulated in Equation (13).

$$T = \int_V \left[\frac{1}{2}\rho \dot{u}_j^l \dot{u}_j^l + \frac{1}{2V'} \gamma^2 \int_{V'} \rho^l \dot{u}_j^n l \dot{u}_j^n l dV' \right] dV \tag{13}$$

The local stresses are calculated with the classical finite element model is used. The local stress data is exported. This discrete data is numerically integrated to obtain the nonlocal stresses. Here, it is important to note that the local strain field is assumed to be the same as the nonlocal strain field and the system is assumed to be weakly nonlocal.

RESULTS

Calculation of Local Stresses

The finite element model is used to calculate the stress and strain distribution of the blade under quasi-static loading. The blade is found to be safe under the prescribed loads and boundary conditions as a result of the quasi-static analysis. In other words, the maximum principal stress is below the standard range of yield

stress values of such materials. However, to evaluate the long-term safety, an extensive research on the fatigue characteristics of the blade structure is required.

Fig. 7 shows the logarithmic maximum principal strain distribution. The maximum logarithmic principal strain is approximately 0.5 %. The strain values increase significantly towards the root around the trailing edge of the blade, especially on the pressure side. For the rest of the blade, the strain field is relatively smooth.

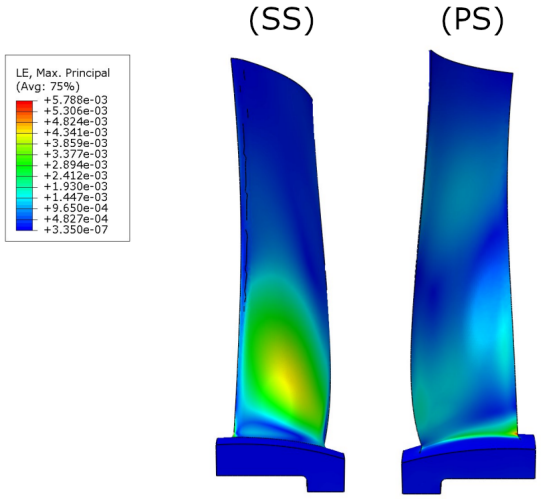

FIGURE 7. LOGARITHMIC MAXIMUM PRINCIPAL STRAIN DISTRIBUTION

Similar comments can be made on the maximum principal stress distribution. The stress distribution is presented in Fig. 8. The stress concentrates around the same region, on the pressure side, around the root, at the trailing edge. The maximum value lies around 638 MPa which is safely below the yield strength of the material Ti–6Al–4V titanium which is supposed to be around 1 GPa [14]. The existence of that stress concentration can be explained with loads and geometry. The centrifugal load causes tension as well as pressure causing bending which leads to more tension on pressure side. Due to the non-uniform pressure distribution and geometry, there is a resultant twisting moment. So there are shear stress components resulting from torsional deformation. In terms of geometry, the trailing edge is sharper than any other edge on this solid model. Higher curvature, of course, creates higher stresses [14]. This combination generates a greater value of principal stress. In the design process of a real fan blade, this stress concentration must have been observed. Therefore, the thickness around the root, and especially at the edges, increase significantly, as shown in Fig. 9.

Furthermore, there is a region on the suction side where relatively higher stresses are observed. This is interpreted to occur due to the higher curvature of the blade which causes stiffer bending behaviour. Additionally, twist introduces shear stress of significant magnitude as well. Therefore, the principal stresses there, are higher, whereas, around the root at the suction side, lower stress values are observed. This is caused by the introduction of stresses of opposite characters by the external loads. The centrifugal loads introduce tension around that region whereas the pressure leads to compression due to bending. These two opposite characteristic of stresses reduce the resultant stress value.

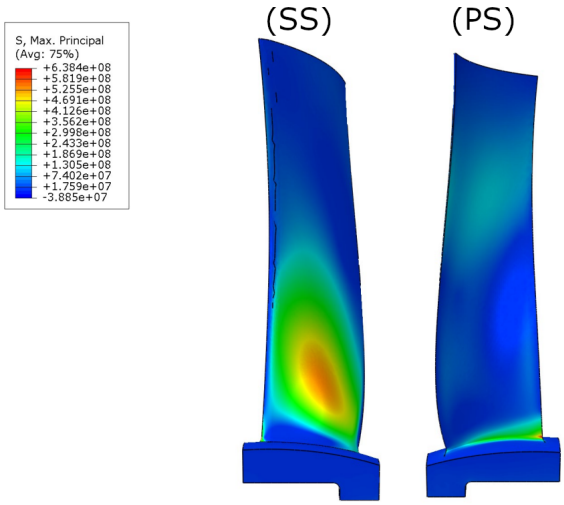

FIGURE 8. LOCAL MAXIMUM PRINCIPAL STRESS DISTRIBUTION (UNITS IN [Pa])

FIGURE 9. THICKNESS CHANGE AROUND THE ROOT

Calculation of Nonlocal Stresses

As explained in some details in the previous section, the chosen attenuation function is plugged into the normalisation equation and the necessary constants are calculated. Fig. 10 is the plotted normalised attenuation function that is used to calculate the nonlocal stresses. This function fulfils each and every condition which is described by the nonlocal continuum theory.

To introduce a practical concept, the expression "influence radius" is used in this paper. This concept describes the maximum distance between the field points and the points of interest, at which the nonlocal attenuation function has practically nonzero values to make significant changes in the resultant nonlocal steess when not included in the integral. It is to be observed that there is a practical influence radius, which is around 2 times the extrinsic length l. To note that l, is chosen as 5 mm based on an average thickness value of the blade. So the radius where this integration makes a significant difference lies about 12.5 mm.

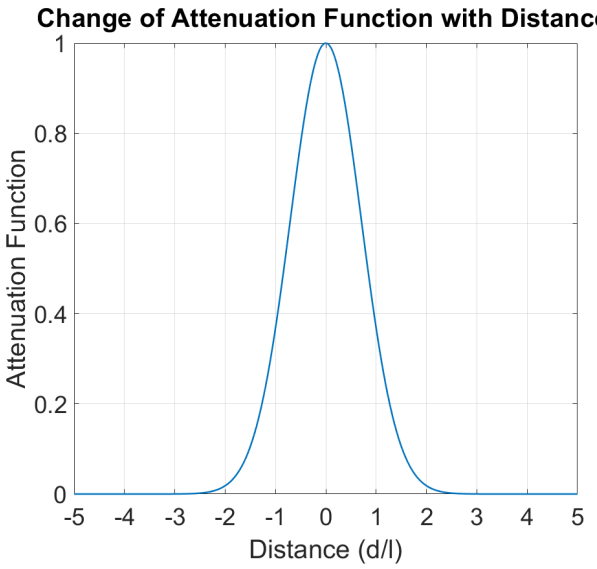

FIGURE 10. NONLOCAL ATTENUATION FUNCTION IN NEAR NEIGHBOURHOOD

The stress data is exported from the finite element simulation of the blade and imported into Python for further processing. The integral given in Equation (4), is discretised and the local stresses are put through that triple integration process being multiplied with the attenuation function. The results, the nonlocal stress components are taken and the maximum principal stresses are calculated. Fig. 11 displays the nonlocal principal stresses.

The distribution is generally similar but the values of stress generally increase. This is visible in Fig. 11. The maximum stress increases more than 20%. The peak of the maximum principal nonlocal stress is calculated as 789 MPa whereas the local respective value is 638 MPa.

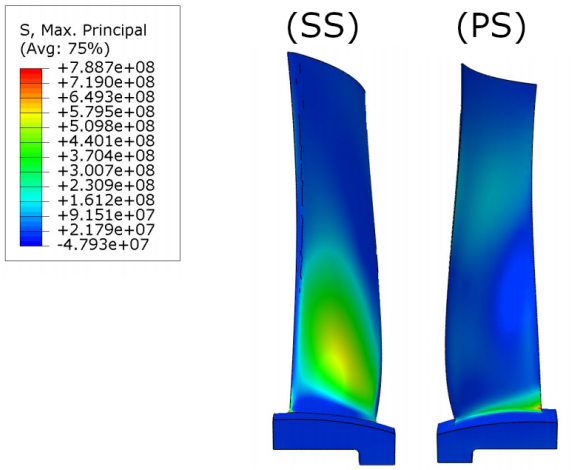

FIGURE 11. NONLOCAL MAXIMUM PRINCIPAL STRESS DISTRIBUTION (UNITS IN [Pa])

It is also to be noted that there is no constant ratio between local and nonlocal stresses, as this is a relatively complicated integral operation. The ratio of nonlocal and local stresses grows with the magnitude of the local stresses. This increases the difference between nonlocal and local stresses around stress concentrations. In other words, the stress concentration factors increase. Fig. 12 displays the maximum principal stress distributions for both local and nonlocal theories around the stress peak near the root on the pressure side. Fig. 13 and 14 are plotted for better visualisation of this fact of this phenomena. The local and nonlocal stress values that are taken from the local finite element points are compared to the nonlocal stresses taken from the same locations. Fig. 13 is taken from the stress concentration region, whereas Fig. 14 is taken from where the stress levels are significantly lower. It is to be seen that the increase is more significant around the stress concentration than a location where stresses are less. This also affects the design of the blade, as the safety inspections are usually done with the maximum values.

Modal Analysis of the Blade

After manipulating the mass properties to improve the accuracy of the nonlocal dynamic calculations and with the obtained nonlocal stress field, it is possible to run some modal analyses on the blade with nonlocal properties. In both, local and nonlocal cases, the stress fields are kept as well as the boundary condi-

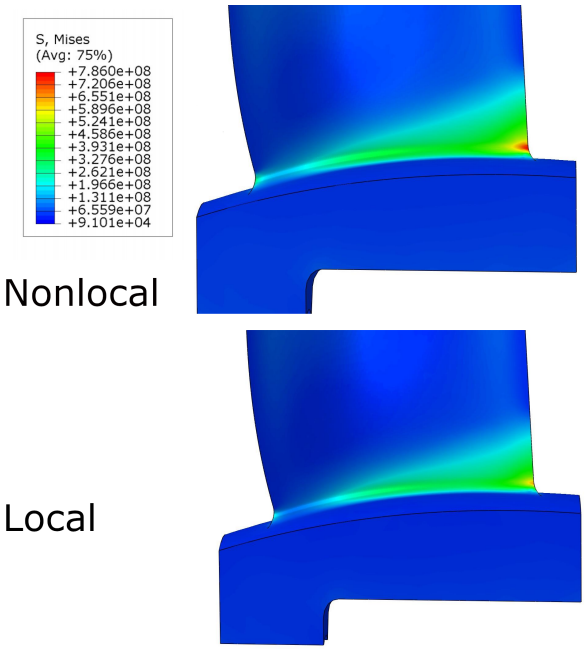

FIGURE 12. COMPARISON OF LOCAL AND NONLOCAL MAXIMUM PRINCIPAL STRESS DISTRIBUTIONS NEAR ROOT STRESS CONCENTRATION (UNITS IN [Pa])

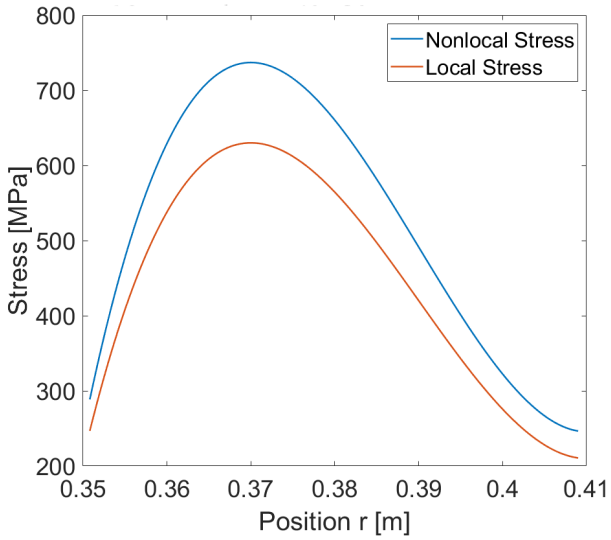

FIGURE 13. COMPARISON OF LOCAL AND NONLOCAL MAXIMUM PRINCIPAL STRESS DISTRIBUTIONS NEAR ROOT STRESS CONCENTRATION

tions. With varying rotational speeds and pressure distributions as the pressure distribution mainly depends on the rotation speed

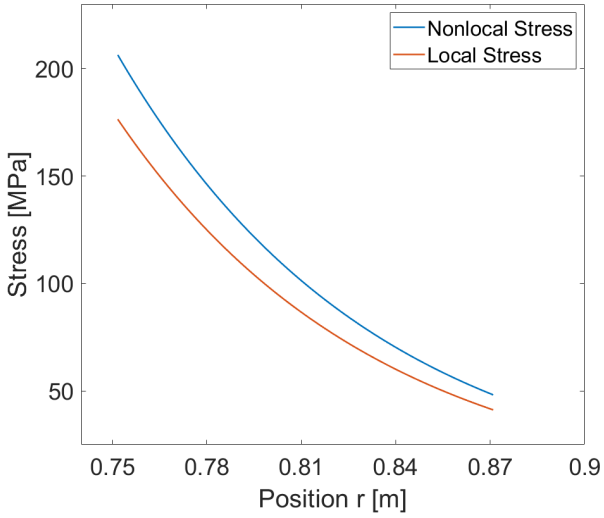

FIGURE 14. COMPARISON OF LOCAL AND NONLOCAL MAXIMUM PRINCIPAL STRESS DISTRIBUTIONS NEAR TIP

of the fan, modal analyses are run. The first five natural frequencies and mode shapes are included in this manuscript. The first five mode shapes of the blade are presented in Fig. 15

The comparison of natural frequencies depending on the rotation speed is presented in Fig. 16. It is to be seen that the frequencies decrease as the nonlocality takes effect. Therefore, the lower natural frequencies belong to the results of calculations with nonlocal theory fields. The nonlocal stiffness and mass matrices both are greater then the local properties. Even though, a frequency shift occurs. This is because of the components of the mass matrix grow more significantly in comparison to the components of the stiffness. Although the difference is approximately between 2 and 5 %. The first This can be explained with the weak nonlocal characteristics of the material considered in this study.

CONCLUSIONS

In this study, the stress and modal analysis of a representative structure of an aero-engine's fan blade is investigated. To do the analyses, local and nonlocal theories are employed and their results are compared.

The nonlocal stresses are obtained by postprocessing the local stresses using the discretised version of the integral equation of the nonlocal continuum theory while the mass properties are manipulated by generating the nonlocal terms and adding those to the classical mass properties.

The first five natural frequencies are found to be slightly lower in nonlocal theory in comparison to the local theory. However, the nonlocal theory calculated the stresses to be relatively

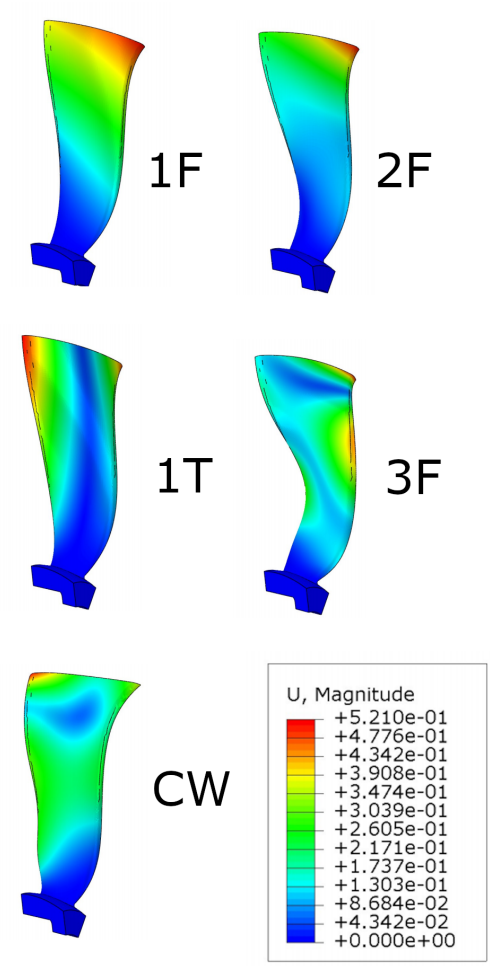

FIGURE 15. MODE SHAPES OF THE BLADE

higher than the local theory. But it crucial to note that the strongly nonlocal a system gets, those changes get more dramatic. Therefore the new generation materials that obey the constitutive laws of nonlocal theory, are to be handled in engineering designs with more care and caution.

In the future, it is planned to investigate the effect of the variation of the nonlocal modulus on the behaviour of the system. It is also aimed to include the nonlocal damping properties for the mechanical systems, as the damping also needs to be reviewed as the mass and stiffness properties. Including damping in engineering calculations is crucial for accurate predictions of mechanical characteristics and behaviour of the systems. Furthermore, frequency-domain modelling is also to be done to be able to analyse the dynamics of nonlocal systems.

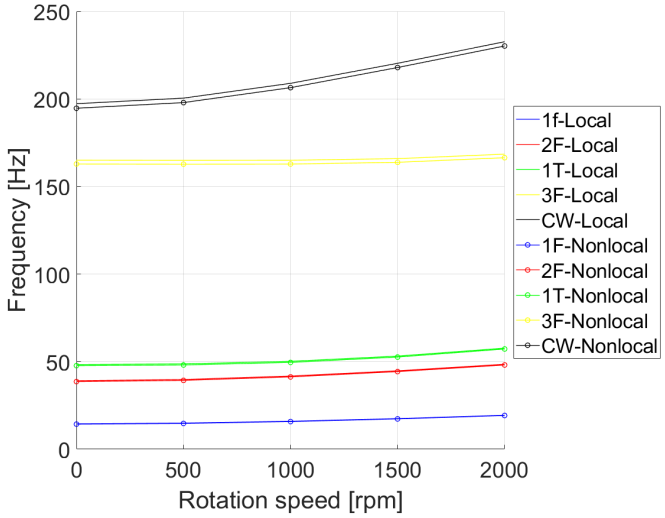

FIGURE 16. COMPARISON OF THE NATURAL FREQUENCIES CALCULATED WITH LOCAL AND NONLOCAL THEORIES

ACKNOWLEDGMENT

The authors would like to acknowledge the support of Scientific and Technological Research Council of Turkey (TUBITAK) that makes this research possible.

REFERENCES

[1] Ghadiri, M., and Shafiei, N., 2017. "Vibration analysis of a nano-turbine blade based on Eringen nonlocal elasticity applying the differential quadrature method". *JVC/Journal of Vibration and Control,* ***23***(19), pp. 3247–3265.

[2] Amoo, L. M., 2013. "On the design and structural analysis of jet engine fan blade structures". *Progress in Aerospace Sciences,* ***60***, pp. 1–11.

[3] Cumpsty, N., 2009. *Jet propulsion*. Cambridge University Press.

[4] Vahdati, M., and Salles, L., 2015. The effects of mistuning on fan flutter.

[5] Salles, L., Blanc, L., Thouverez, F., Gouskov, A. M., and Jean, P., 2009. "Dynamic analysis of a bladed disk with friction and fretting-wear in blade attachments". In Proceedings of the ASME Turbo Expo.

[6] Liu, Z., Chen, Z., and Chen, J., 2018. "The Strength Analysis of CFM56 Engine Blade". *MATEC Web of Conferences,* ***166***, pp. 2–5.

[7] jun Kou, H.-j., sheng Lin, J.-S., hong Zhang, J.-H., and Fu, X., 2017. "Dynamic and fatigue compressor blade characteristics during fluid-structure interaction: Part I—Blade modelling and vibration analysis". *Engineering Failure Analysis,* ***76***, pp. 80–98.

[8] Chahine, C., Verstraete, T., and He, L., 2015. "Multidisciplinary design optimization of an aero-engine fan blade with consideration of bypass and core performance". In Proceedings of the 11th World Congress on Structural and Multidisciplinary Optimization, no. June, pp. 5–10.

[9] Leissa, A. W., Lee, J. K., and Wang, A. J., 1981. "Rotating blade vibration analysis using shells". *Proceedings of the ASME*, pp. 1–8.

[10] Yucel, A., Arpaci, A., and Tufekci, E., 2014. "Coupled axial-flexural-torsional vibration of Timoshenko frames". *JVC/Journal of Vibration and Control,* ***20***(15), pp. 2366–2377.

[11] Tufekci, E., Eroglu, U., and Aya, S. A., 2017. "A new two-noded curved beam finite element formulation based on exact solution". *Engineering with Computers,* ***33***(2), pp. 261–273.

[12] Rand, O., 1995. "Experimental study of the natural frequencies of rotating thin-walled composite blades". *Thin-Walled Structures,* ***21***(2), pp. 191–207.

[13] Yuan, J., Allegri, G., Scarpa, F., Rajasekaran, R., and Patsias, S., 2015. "Novel parametric reduced order model for aeroengine blade dynamics". *Mechanical Systems and Signal Processing,* ***62***(March), pp. 235–253.

[14] Carney, K. S., Pereira, J. M., Revilock, D. M., and Matheny, P., 2009. "Jet engine fan blade containment using an alternate geometry". *International Journal of Impact Engineering,* ***36***(5), pp. 720–728.

[15] Zhou, J., Liu, J., Zhang, X., Yan, Y., Jiang, L., Mohagheghian, I., Dear, J. P., and Charalambides, M. N., 2019. "Experimental and numerical investigation of high velocity soft impact loading on aircraft materials". *Aerospace Science and Technology,* ***90***, pp. 44–58.

[16] Xiao, J., Chen, Y., Zhu, Q., Lee, J., and Ma, T., 2017. "A general ply design for aero engine composite fan blade". *Proceedings of the ASME Turbo Expo,* ***7A-2017***, pp. 1–8.

[17] Wollmann, T., Dannemann, M., Langkamp, A., Modler, N., Gude, M., Salles, L., and Hoffmann, N., 2018. "Combined Experimental-Numerical Approach for the 3D Vibration Analysis of Rotating Composite Compressor Blades : an Introduction". In 18th European Conference on Composite Materials, no. June, pp. 24–28.

[18] Ávila, A. F., 2000. "Integrated micro/macro approach for laminate composite analysis: Applications to turbine blades". *AIAA journal,* ***38***(10), pp. 1924–1930.

[19] Polizzotto, C., Fuschi, P., and Pisano, A. A., 2006. "A nonhomogeneous nonlocal elasticity model". *European Journal of Mechanics, A/Solids,* ***25***(2), pp. 308–333.

[20] Gulmez, D. E., Yildiz, Y. O., and Kirca, M., 2018. "Nanoporous gold reinforced with carbon based nanomaterials: A molecular dynamics study". *Composites Part B: Engineering,* ***151***(65), pp. 62–70.

[21] Monetto, I., and Drugan, W. J., 2009. "A micromechanics-based nonlocal constitutive equation and minimum RVE size estimates for random elastic composites containing aligned spheroidal heterogeneities". *Journal of the Mechanics and Physics of Solids,* ***57***(9), pp. 1578–1595.

[22] Li, L., Tang, H., and Hu, Y., 2018. "Size-dependent nonlinear vibration of beam-type porous materials with an initial geometrical curvature". *Composite Structures,* ***184***, pp. 1177–1188.

[23] Mindlin, R. D., 1964. "Micro-structure in Linear Elasticity". *Archive Rational Mechanical Analysis,* ***16***, pp. 51–78.

[24] Eringen, A. C., and Edelen, D. G. B., 1972. "On nonlocal elasticity". *International Journal of Engineering Science,* ***10***(3), pp. 233–248.

[25] Eringen, A. C., 2002. *Nonlocal Continuum Field Theories*. Springer.

[26] Eringen, A. C., 1983. "On differential equations of nonlocal elasticity and solutions of screw dislocation and surface waves". *Journal of Applied Physics,* ***54***(9), pp. 4703–4710.

[27] Aydogdu, M., 2012. "Longitudinal wave propagation in nanorods using a general nonlocal unimodal rod theory and calibration of nonlocal parameter with lattice dynamics". *International Journal of Engineering Science,* ***56***, pp. 17–28.

[28] Tufekci, E., Aya, S. A., and Oldac, O., 2016. "A unified formulation for static behavior of nonlocal curved beams". *Structural Engineering and Mechanics,* ***59***(3), pp. 475–502.

[29] Tufekci, E., and Aya, S. A., 2018. *Nonlocal Continuum Modeling of Curved Nanostructures*. Elsevier Inc.

[30] Aydogdu, M., 2009. "Axial vibration of the nanorods with the nonlocal continuum rod model". *Physica E: Low-Dimensional Systems and Nanostructures,* ***41***(5), pp. 861–864.

[31] Savelyeva, I. Y., Cherednichenko, A. V., and Shukhtin, A. P., 2019. "Stress-strains state calculation of a rod at uniaxial tension with non-local effects". *IOP Conference Series: Materials Science and Engineering,* ***489***(1).

[32] Tufekci, E., Eroglu, U., and Aya, S. A., 2016. "Exact solution for in-plane static problems of circular beams made of functionally graded materials". *Mechanics Based Design of Structures and Machines,* ***44***(4), pp. 476–494.

[33] Pisano, A. A., Sofi, A., and Fuschi, P., 2009. "Nonlocal integral elasticity: 2D finite element based solutions". *International Journal of Solids and Structures,* ***46***(21), pp. 3836–3849.

[34] Pisano, A. A., Sofi, A., and Fuschi, P., 2009. "Finite element solutions for nonhomogeneous nonlocal elastic problems". *Mechanics Research Communications,* ***36***(7), pp. 755–761.

[35] Fuschi, P., Pisano, A. A., and De Domenico, D., 2015. "Plane stress problems in nonlocal elasticity: Finite element solutions with a strain-difference-based formula-

tion". *Journal of Mathematical Analysis and Applications,* ***431***(2), pp. 714–736.

[36] Lefebvre, L. P., Banhart, J., and Dunand, D. C., 2008. "Porous metals and metallic foams: Current status and recent developments". *Advanced Engineering Materials,* ***10***(9), pp. 775–787.

[37] Davies, G. J., and Zhen, S., 1983. "Metallic foams: their production, properties and applications". *Journal of Materials Science,* ***18***(7), pp. 1899–1911.

[38] Sayma, A., Vahdati, M., and Imregun, M., 2001. "An integrated nonlinear approach for turbomachinery forced response prediction. part i: Formulation". *Journal of Fluids and Structures,* ***15***(1), pp. 1–13.

[39] Tufekci, M., Koc, H., Genel, O. E., and Oldac, O., 2018. "Free Transverse Vibrations of Rotating Annular Disks Under Various Boundary Conditions". *Sigma Journal of Engineering and Natural Sciences,* ***9***(2), pp. 243–255.

[40] Tuna, M., and Kirca, M., 2016. "Exact solution of Eringen's nonlocal integral model for vibration and buckling of Euler–Bernoulli beam". *International Journal of Engineering Science,* ***107***, pp. 54–67.

[41] Murmu, T., and Adhikari, S., 2010. "Nonlocal effects in the longitudinal vibration of double-nanorod systems". *Physica E: Low-Dimensional Systems and Nanostructures,* ***43***(1), pp. 415–422.